Physica Scripta. Vol. T67, 7–11, 1996

Competition and Coexistence of Two-Dimensional Optical Patterns

F. T. Arecchi,* S. Boccaletti,* E. Pampaloni, P. L. Ramazza and S. Residori

Istituto Nazionale di Ottica, 50125 Firenze, Italy
* also Phys. Dept., University of Florence, Italy

Received December 5, 1995; accepted April 22, 1996

Abstract

We report experimental evidence of temporal coexistence and alternation of patterns having different scales in a nonlinear optical system formed by a Kerr-like medium with feedback. Time coexistence occurs via spatial segregation of the different patterns in different domains, separated by topological defects.

A simple theoretical model yields predictions in good agreement with the experimental results.

1. Introduction

Pattern forming instabilities are a rather general phenomenon in spatially extended systems driven out of thermodynamical equilibrium [1–3]. In general, patterns of different symmetry and/or characteristic scale can occur at different threshold values of some control parameter. Close to the lowest threshold only one kind of structures can be observed, namely the one associated with the most unstable mode.

If the control parameter is increased to a value that allows for more than one pattern above threshold, some general scenarios have been identified. Among these we recall mode alternation in time (either periodic or chaotic) [4–6], domination of one mode over the others [7, 8] and mode-mode coexistence [5, 9, 10].

In this paper we report experimental evidence of pattern alternation in time and of pattern coexistence in an experiment consisting of a Kerr-like medium inserted in an optical feedback loop. Two-dimensional patterns having different spatial scales are shown to coexist in time, but segregated in spatially separated domains. The one-dimensional analog of this phenomenon was demonstrated in hydrodynamical convection [11], and has been object of a recent theoretical treatment [12].

The presence of topological defects in our system is closely connected both with pattern alternation and with pattern coexistence in different domains. A simple model where the role of defects is reduced to a noise term gives an explanation of the main features of the experiments reported here.

2. Experimental results

The system used in the experiments consists of a Liquid Crystal Light Valve (LCLV) inserted in an optical feedback loop [13] as shown in Fig. 1(a). A schematic drawing of the LCLV is shown in Fig. 1(b). This device consists essentially of a nematic liquid crystal cell, a dielectric mirror and a photoconductive layer. A supply voltage V_0 is applied by means of transparent electrodes to the series of these three elements. The liquid crystal birefringence is a monotonic decreasing function of the voltage drop V_{LC} across it [14]. Since the liquid crystal and the photoconductor are placed

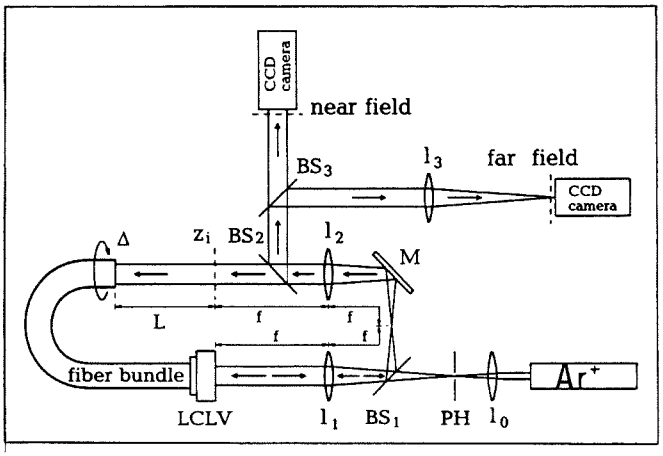

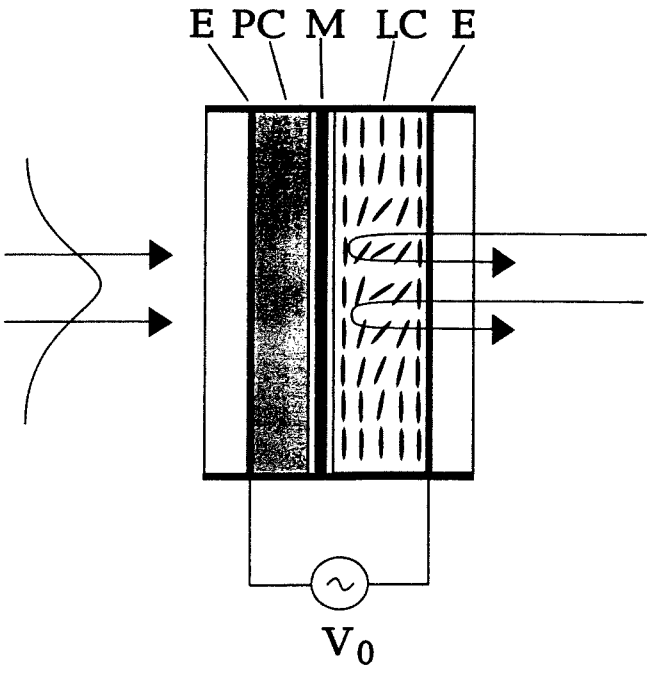

Fig. 1. (a) Experimental setup; l_i = lens, M = mirror, BS_i = beamsplitters, PH = pinhole, L = free propagation length, Δ = feedback rotation angle; (b) Liquid Crystal Light Valve (LCLV): LC = liquid crystal layer, M = mirror, PC = photoconductor layer, E = transparent electrodes, V_0 = applied AC voltage. The liquid crystal molecules re-orient according to the write intensity incident on the PC.

in series, the fraction V_{LC} of the total voltage V_0 will increase when the writing illumination incident on the photoconductive layer increases. It follows that a writing beam impinging on the rear side of the LCLV induces a variation in the extraordinary index of refraction of the liquid crystals. This variation is of negative sign and in first approximation proportional to the writing intensity, so that the LCLV can be considered as a defocussing Kerr medium.

In our experimental set up a beam from an He-Ne laser operating at 632 nm is spatially filtered and expanded by means of the telescopic system formed by lenses l_0 and l_1 and pinhole PH. The resulting plane wave, that is polarized along the extraordinary axis of the liquid crystal, is sent on the front face of the LCLV. The wave reflected by the LCLV acquires a spatial phase modulation, which is determined by the distribution of the extraordinary index of refraction n in the liquid crystal layer. The front plane of the LCLV is imaged onto plane z_i by means of lenses l_1 and l_2. Along the image forming path, a fraction of the beam is extracted at the beam splitter BS_2 and used for detection of the near and far field signal. From plane z_i to the input plane z_2 of the fiber bundle the wave undergoes a free propagation path of length L. At plane z_2 the diffracted wave enters an optical fiber bundle, that just relays the intensity distribution from its input to its output plane. This last one is in contact with the rear face of the LCLV.

The origin of pattern formation in a system of this kind lies on the following mechanism [15]. The perturbations of the index of refraction n in the liquid crystal layer induce a phase modulation on the reflected beam. This phase modulation is converted into amplitude modulation, by diffractive propagation along L. The light intensity reaching the rear side of the LCLV provides via the Kerr effect a feedback on the perturbations of n.

In the experiment reported here, we adjust the LCLV voltage at 12.3 Volts r.m.s and 3 kHz, the free propagation length at $L = 10$ cm and the angle of rotation of the fiber at $\Delta = 2\pi/7$. In these conditions, the linear stability analysis [16] predicts that, as the incident intensity I_0 overcomes I_{th}, the first unstable wavenumber is $q_2 = 2\pi\sqrt{3}/\sqrt{2\lambda L}$. This is indeed observed experimentally, as shown in Fig. 2(a). The patterns shown here display a quasicrystalline structure, as discussed in [16].

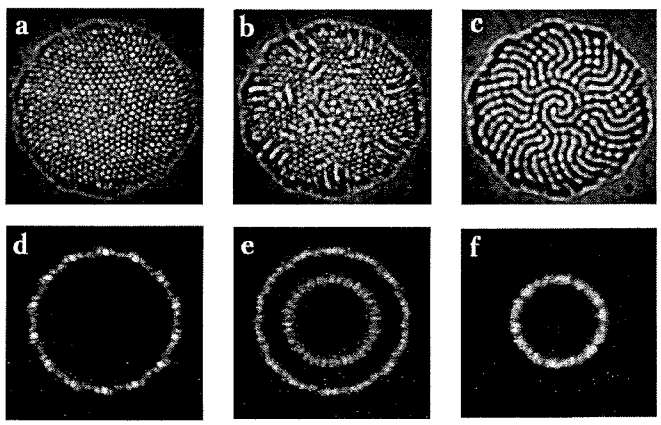

Fig. 2. Near field (upper) and far field (lower) patterns observed for $\varepsilon = 0.5$ (a, d), $\varepsilon = 2$ (b, e) and $\varepsilon = 4.2$ (c, f). Left (right) column corresponds to excitation of only the q_2 (q_1) band, in the middle column the two bands coexist. The single wavenumber cases (left and right) show coexistence of many sets of $2N = 14$ vectors.

Let us define a reduced pump parameter $\varepsilon = (I_0 - I_{th})/I_{th}$. For very small ε, a single q band is associated with a far field made of $2N$ spots (fixed orientation of the wavevectors) and hence the near field shows mainly a single domain (besides some boundary perturbations) [16]. On the contrary, here (rather larger ε) even a single band is a collection of wavevectors with different orientations, and hence even for a single wavelength we have a many-domain pattern, with grain boundaries separating different orientations.

A gradual increase of ε starting from $\varepsilon = 0$ leads initially to an increase of the amplitude of the quasicrystalline patterns, without a scale change. A further increase in ε results in the destabilization of a second band at $q_1 = 2\pi/\sqrt{2\lambda L}$ [Fig. 2(b)]. In this situation the near field signal does not appear as a uniform superposition of patterns at the two different wavelengths, but rather as a collection of spatially separated domains, each one containing patterns at only one of the two spatial scales. Domains with the smaller wavenumber q_1 emerge at the grain boundaries of the previous q_2 multi-orientation patterns, thus showing that defects are sources that trigger the onset of the q_1 patterns. The average size of the domains with $q = q_1$ increases for increasing ε and eventually the whole wavefront is made of domains at this wavenumber, while the domains at $q = q_2$ are completely suppressed [Fig. 2(c)].

In Fig. 3 we report the local intensities at one point of the near field for the three cases described above. When wavenumber q_2 is excited ($\varepsilon = 0.2$) we have relatively slow drifts of the domain boundaries. When only q_1 is excited ($\varepsilon = 4.5$) the corresponding eigenvalue λ is complex [16] and thus we obtain rotating patterns. The rotation gives rise to a high frequency as observed in Fig. 3(c). Finally in Fig. 3(b) ($\varepsilon = 1.9$) the two wavenumbers coexist and at a given pixel we have an alternation between the two regimes.

Further information about the observed phenomena can be gained from the spatial power spectra of the signal, corresponding to the far field. Typical examples of these spectra are shown in Fig. 2(d–f). In order to obtain some global information about the temporal behavior of the signal, we

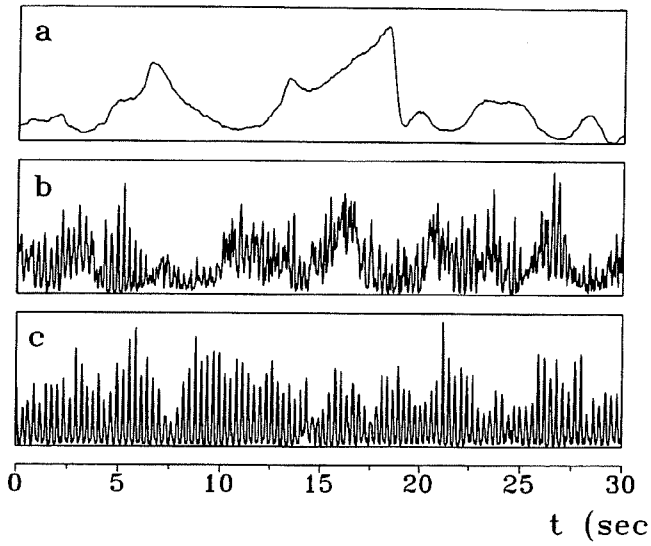

Fig. 3. Near field local intensity (arbitrary units) *vs.* time. In a) ($\varepsilon = 0.2$, q_2 band) the fluctuations are due only to domain dynamics; in c) ($\varepsilon = 4.5$, q_1 band) there is also a fast oscillation due to the imaginary part of the eigenvalue; in b) ($\varepsilon = 1.9$, both q_1 and q_2 bands) there is a superposition of the other two cases.

define the quantity $\eta(t) = S_1(t)/(S_1(t) + S_2(t))$ as the fraction of the total power that instantaneously belongs to the first band. Here $S_j(t)$ $(j = 1, 2)$ is the instantaneous power radially integrated in the Fourier space over a circular corona of radius q_j. A plot of $\eta(t)$ for three different values of ε is shown in Fig. 4. It is seen here that, when the system is dominated by one of the two competing bands, the time fluctuations of $\eta(t)$ are very small. On the contrary, the range of ε for which the two bands show coexistence corresponds to regions of high fluctuation for $\eta(t)$, meaning that there neither the coexistence of the two bands nor the domination of one band over the other are stable phenomena.

A quantitative measurement of the transition from the band q_2 to the band q_1 dominated regime is given by the behavior of the time average $\bar{\eta}\langle\eta(t)\rangle_t$ and of the standard deviation $\sigma \equiv [\langle\bar{\eta}^2 - \eta(t)^2\rangle_t]^{1/2}$ of the quantity $\eta(t)$, *vs.* the pump parameter ε. Plots of the results of these measurements are shown in Fig. 5 (left). These plots give a quantitative confirmation of the enhancement of fluctuations in the signal that accompanies the regimes of competition-coexistence between the two bands. In the next section we will explain the criteria that give rise to the theoretical plots reported on the right of Fig. 5.

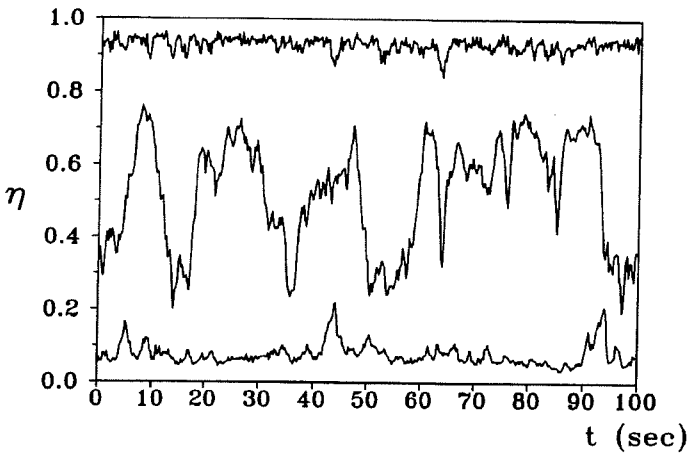

Fig. 4. Temporal evolution of the normalized spectral power η on the first ring. $\varepsilon = 1$, q_2 band (lower curve), $\varepsilon = 4.1$, q_1 band (upper curve) and $\varepsilon = 2.1$, both q_1 and q_2 bands (middle curve).

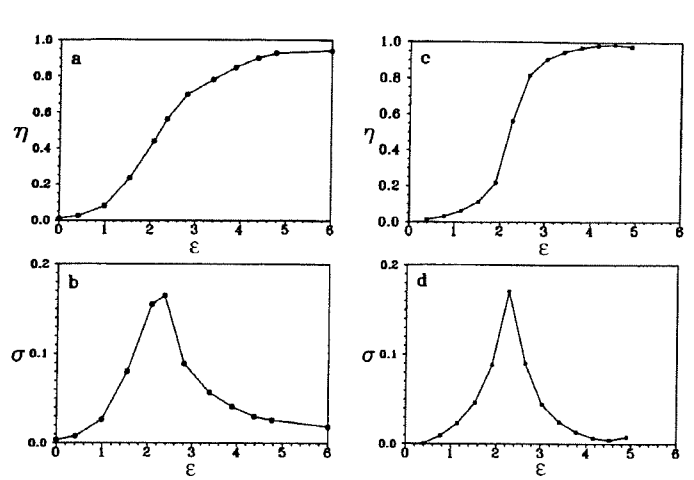

Fig. 5. Experimental (left column) and theoretical (right column) plots of $\eta(\varepsilon)$ (a, c) and $\sigma(\varepsilon)$ (b, d). Experimental error bars are within the size of the black circles. Theoretical points (black squares) are obtained from numerical integration of eq. (3) with $\mu_1 = 1 - (I_0 - 5)^2$, $\mu_2 = 1 - (I_0 - 5.5)^2$, $\beta_1 = \beta_2 = 1.5$, $\gamma_1 = \gamma_2 = 2.4$ and the noise addition. The x axis has been normalized to the reduced pump parameter ε. In all cases, lines are just a guide connecting points.

3. The theoretical model

The coupled field-nonlinear medium dynamics is ruled by two partial differential equations (1) and (2). Equation (1) describes the dissipative-diffusive reorganization of the refractive index $n(x, y)$ in a thin cell (thickness d much smaller than the diffusive length $l_d = \sqrt{D\tau}$, where D and τ are defined by the same eq. (1)) as

$$\left(\partial_t + \frac{1}{\tau} - D\nabla^2\right)n = -\chi|E_w|^2 \tag{1}$$

Here ∇^2 is the (x, y) Laplacian, $\chi > 0$ (defocussing medium) is a constant and E_w (w for writing) is the field impinging onto the photoconductor back of the LCLV.

The electromagnetic equation in the eikonal approximation is given by

$$\left(\partial_z + \frac{\mathrm{i}}{2k}\nabla^2\right)E = inE \text{ rect } (z/d), \tag{2}$$

where rect $(\xi) \equiv 1(0)$ for $\xi < 1(> 1)$. In eq. (2) the nonlinear r.h.s. is limited by the rect function to a length d around $z = 0$, z being the longitudinal coordinate along the axis of the optical system, and the time derivative is neglected since the transit time along the feedback loop (10^{-7} s) is much faster than the characteristic time of the refractive medium ($\tau \times 10^{-2}$ s). Solution of eq. (2) for an impinging field E_0 gives a field E_1 exiting the Kerr cell given by

$$E_1 = E_0 \mathrm{e}^{ind}, \tag{3}$$

since diffraction plays no role over the distance d. This field freely propagates, providing an input E_2 to the fiber bundle, which is symbolically written in terms of an operator corresponding to a formal integration of eq. (2) as

$$E_2 = \mathrm{e}^{-\mathrm{i}(L/2k)\nabla^2}E_1. \tag{4}$$

The diffraction operator becomes a simple phase factor in the $\boldsymbol{q}$ space, where $\boldsymbol{q}$ is the Fourier transform of the (x, y) dependence.

The azimuthal rotation within the fiber bundle corresponds to applying a rotation operator $R(\Delta)$ to the field E_2. Thus we have

$$|E_w|^2 = |R(\Delta)E_2|^2. \tag{5}$$

Combining eqs (3)–(5) into eq. (1) we arrive at a single closed, but non-local and highly nonlinear, equation for $n(x, y)$ with a source term

$$|E_w(r, \theta)^2 = I_0|\mathrm{e}^{-\mathrm{i}(L/2k_0)\nabla^2}\mathrm{e}^{in(r,\,\theta+\Delta)}|^2, \tag{6}$$

where $I_0 \equiv |E_0|^2$, and (r, θ) are polar coordinates in the transverse plane.

The experimental observations reported in Fig. 2 are performed in the near field E_2 (after diffractive propagation) and in its Fourier transform (far field).

In Ref. [16] we have linearized the above problem, and found the instability conditions. Working close to threshold, we were able to give evidence of different classes of two-dimensional symmetries.

Suppose that the homogeneous solution is perturbed by a phase modulation of wavevector $\boldsymbol{q}$ and that the feedback rotation of an angle $\Delta = 2\pi/N$ excites N vectors with the same length in N directions spaced by the angle Δ. Therefore, the phase perturbation can be expanded as $n = \sum_{j=1}^{N} a_j \cos \boldsymbol{q}_j \cdot \boldsymbol{r}$. The $\boldsymbol{q}$ vectors are related by the rotation operator in such a way that

$$R\boldsymbol{q}_j = \boldsymbol{q}_{j+1}. \tag{7}$$

With this expansion, the propagation over a distance L of a field gives rise to the following feedback intensity

$$|E_2(L, \boldsymbol{r})|^2 = I_0\left(1 + \sin \frac{q^2 L}{2k_0} \sum_{j=1}^{N} a_j \cos \boldsymbol{q}_j \cdot \boldsymbol{r}\right). \tag{8}$$

Using eq. (5) and substituting this expression into eq. (1), we evaluate the eigenvalues λ_j of the perturbation vector $(a_1, a_2, \ldots, a_N)$ as

$$\lambda_j = -(1 + l_D^2 q^2) + \chi I_0 \sin q^2 L/2k_0 [e^{iN\pi}]_j^{1/N} \tag{9}$$

where $[\ ]_j^{1/N}$ denotes the jth Nth root of the unity. By selecting the eigenvalues with maximal real parts, we derive two marginal stability curves
branches I:

$$\chi I_{\text{th}} = \begin{cases} \dfrac{1 + l_D^2 q^2}{\sin (q^2 L/2k_0)} & \text{for } N \text{ even}, \\ \dfrac{1 + l_D^2 q^2}{\cos (\Delta/2) \sin (q^2 L/2k_0)} & \text{for } N \text{ odd}, \end{cases} \tag{10}$$

branches II:

$$\chi I_{\text{th}} = -\frac{(1 + l_D^2 q^2)}{\sin \dfrac{q^2 L}{2k_0}} \quad \text{for } N \text{ even or odd}. \tag{11}$$

The positive branches of these two curves give the value I_{th} of the input intensity I_0 necessary to excite an instability with a spatial frequency q. In the diffractive limit, $l_D^2 \ll \lambda L$, all branches have their minima at $q^2 L/2k_0 = (2n + 1)\pi/2$ with $n = 0, 2, \ldots$ (even integer) for branches I and $n = 1, 3, \ldots$ (odd integer) for branches II, so that, with respect to the first critical wavenumber $q_{\text{I}} = \sqrt{\pi k_0/L}$, the next is located at $q_{\text{II}} = \sqrt{3}\, q_{\text{I}}$ and the higher ones at $\sqrt{5}\, q_{\text{I}}, \sqrt{7}\, q_{\text{I}}, \ldots$ Close to threshold, only the first two branches of I and II [reported in Fig. 6(a)] are involved in the wavenumber selection process since they have the lowest minima. Furthermore, for N odd, branch I depends on N through Δ, hence its minimum can be above or below that of branch II. At threshold, the lowest local minimum determines the excited mode.

Comparing the magnitude of the real parts of the two unstable eigenvalues, it results that for N even the excited mode is always the one with q_{I}, independently of N. On the other hand, for N odd branch I has an enhancement factor $1/\cos(\Delta/2)$ (see eq. (10)) which is larger for lower N, as shown for $N = 3$ in Fig. 6(b), and hence branch II is favoured, whereas for high values of N it exists a pair of eigenvalues closest to the real axis, for which branch I can still have the lower threshold.

To deal with competition we must introduce nonlinearities. We do that by accounting for the leading nonlinearities and truncating the Fourier spectrum by a Galerkin procedure.

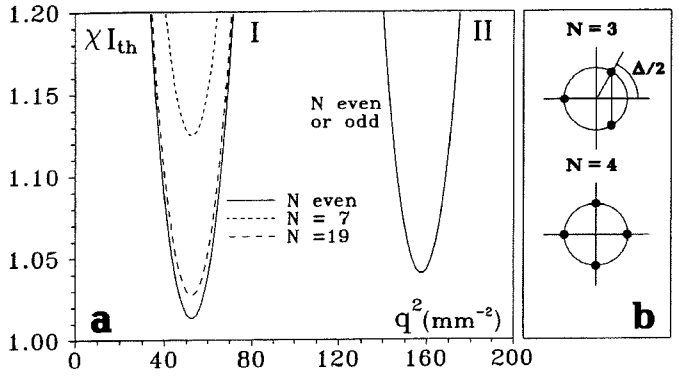

Fig. 6. (a) Marginal stability curves evaluated for $L = 75$ cm and $l_D = 15.5\ \mu$m. The first branch has the lowest threshold for any N if N is even and also for N odd if N is large. For N odd and small the second branch has a lower threshold; (b) The N roots of the unity in the complex plane, for $N = 3$ and 4. For $N = 3$ it is easy to realize the enhancement factor $1/\cos(\Delta/2)$ reported in eq. (10) for N odd.

Let us consider the Fourier expansion of the local optical field on the rear face of the LCLV, corresponding to the observation plane:

$$E(r, t) = \int \mathrm{d}\boldsymbol{q} a_{\boldsymbol{q}}(\tilde{r})\, e^{i\boldsymbol{q} \cdot \boldsymbol{r}} \tag{12}$$

where

$$a_{\boldsymbol{q}}(\tilde{r}) = \sum_{n=1}^{2N} a_n \delta_{\boldsymbol{q} - \boldsymbol{q}_n(\tilde{r})}. \tag{13}$$

The discretization in the set of the Fourier amplitudes is imposed in the experiment by the rotation introduced in the feedback loop and by the recursive relation (7). We are in presence of two active rings in the Fourier space, corresponding to the two unstable values of q.

The mode coupling within one ring (at constant q modulus) was treated in [17], and for $N \neq 3l$ (l being a positive integer) the quadratic nonlinearity disappears by closure considerations, thus leaving a cubic mode coupling of the type considered in laser theory for population coupling in the absence of phase coupling [18]. This applies to our case since we have selected $N = 7$.

The data of Fig. 2 show that a situation of almost isotropic amplitude distribution on the two rings is easily reached. Even though the far field displays this isotropy, the closure relations in building the quadratic convolution term for the evolution equation of $a_q(\tilde{r}, t)$ must be built with a unique set of $2N$ vectors. This rules out the possibility of having $\boldsymbol{q}_i^{\text{I}} + \boldsymbol{q}_i^{\text{II}} = \boldsymbol{q}_j$ ($i \neq j$, i and $j = 1, 2$) since with $N = 7$ ($2N = 14$) points regularly spaced over each ring) and with the ratio $|q_2|/|q_1| = \sqrt{3}$, the above relations are never satisfied. Thus, also the inter-ring competitions are ruled only by cubic nonlinearities. We find it convenient to follow the evolution of the corresponding integrated spectral powers $S_i = 2\pi q_i |a_{qi}|^2$ ($i = 1, 2$). The equations for S_1 and S_2 are

$$\dot{S}_1 = \mu_1 S_1 - \beta_1 S_1^2 - \gamma_1 S_1 S_2,$$
$$\dot{S}_2 = \mu_2 S_2 - \beta_2 S_2^2 - \gamma_2 S_1 S_2. \tag{14}$$

We have thus arrived at general equations well known for competing populations [19] and already used in laser dynamics for two mode operation [18].

Due to the saturating characteristic of the LCLV [20], the linear growth rates μ_i depend on the input intensity I_0. The function $\mu_i(I_0)$ is increasing for moderate I_0 and decreasing for high I_0, where saturation of LCLV characteristic is effective. We choose as a functional form for $\mu_i(I_0)$ a parabola, that is $\mu_i = \alpha_i I_0 - \rho_i I_0^2$, $i = 1, 2$.

The system (14) admits the following four fixed points:

$$O = (0, 0), \quad F1 = \left(\frac{\mu_1}{\beta_1}, 0\right), \quad F2 = \left(0, \frac{\mu_2}{\beta_2}\right)$$

and

$$C = \left(\frac{\mu_1\beta_2 - \gamma_1\mu_2}{\beta_1\beta_2 - \gamma_1\gamma_2}, \frac{\beta_1\mu_2 - \gamma_2\mu_1}{\beta_1\beta_2 - \gamma_1\gamma_2}\right).$$

The spatial interaction neglected in eq. (14) permits the birth of coherent F1 or F2 domain structures, nucleating from local defects. Indeed, when a single family locally displays a defect, this becomes a nucleation center for the other family. Hence, the observed sharing process on the near field can be interpreted as a continuous nucleation and competition of the two coherent domains, and it can be modeled by adding $\mu_2\xi(t)$ and $\mu_1\xi(t)$ to the first and second of eq. (13) respectively, where $\xi(t)$ is a wide band stochastic process with zero average. The noise contribution in the S_1 equation has been multiplied by μ_2 to account for the fact that the perturbation to S_1 arises from S_2 domains nucleating from local defects, hence it is proportional to the growth rate of the second family. Similar considerations hold for the S_2 equation.

In Fig. 5 (right) we report the plots of $\eta(\varepsilon)$ and of $\sigma(\varepsilon)$ extracted from the numerical solutions of eq. (14) with the noise addition. For a suitable choice of parameters, they are in good qualitative agreement with the experiment.

We conclude that the interband dynamics implies both competitive deterministic terms, as well as a stochastic force modelling defect nucleation. In fact a better model, rather than relying on a noise source, should account for the deterministic character of the underlying dynamics. However it has become costumarily, in a many mode dynamics, to account for the perturbation that the modes below threshold induce on the modes already unstable in terms of a suitable noise source [4].

Acknowledgements

Work partly supported by EEC contracts n. CI1*CT93-0331 and CHRX-Ct93-0107.

References

1. Cross, M. and Hohenberg, P. C., Rev. of Mod. Phys. **65**, 851 (1993).
2. "Nonlinear Dynamics and Spatial Complexity in Optical Systems" (Edited by R. G. Harrison and J. S. Uppal) (SUSSP Publications, Edinburgh, and Institute of Physics Publishing, London, 1993).
3. Arecchi, F. T., Il Nuovo Cimento **107A**, 1111 (1994).
4. Ikeda, K., Matsumoto, K. and Otsuka, K., Progr. Theor. Phys., Suppl. n. **99**, 295 (1989).
5. Arecchi, F. T., Giacomelli, G., Ramazza, P. L. and Residori, S., Phys. Rev. Lett. **65**, 2531 (1990).
6. Mandel, P., Georgiou, M., Otsuka, K. and Pieroux, D., Opt. Comm. **100**, 341 (1993).
7. Benkert, C. and Anderson, D. Z., Phys. Rev. **A44**, 4633 (1991).
8. Vorontsov, M. A. and Firth, W. J., Phys. Rev. **A49**, 2891 (1994).
9. Ciliberto, S., Pampaloni, E. and Perez-Garcia, C., Phys. Rev. Lett. **61**, 1198 (1988).
10. Dangoisse, D., Hennequin, D., Lepers, C., Lovergnaux, E. and Glorieux, P., Phys. Rev. **A46**, 5955 (1992).
11. Hegseth, J., Vince, J. M., Dubois, M. and Berge', P., Europhys. Lett. **17**, 413 (1992).
12. Raitt, D. and Riecke, H., Physica **D82**, 79 (1995).
13. Akhmanov, S. A., Vorontsov, M. A. and Ivanov, V. Yu., J. Exp. Theor. Phys. Lett. **47**, 707 (1988).
14. De Gennes, P. G., "The Physics of Liquid Crystals" (Oxford University Press, Oxford 1974).
15. Firth, W. J., J. Mod. Opt. **37**, 151 (1990); D'Alessandro, G. and Firth, W. J., Phys. Rev. Lett. **66**, 2597 (1991).
16. Pampaloni, E., Ramazza, P. L., Residori, S. and Arecchi, F. T., Phys. Rev. Lett. **74**, 258 (1995).
17. Malomed, B. A., Nepomnyaschiĭ, A. A. and Tribelskiĭ, M. I., Sov. Phys. JETP **69**, 388 (1989).
18. Lamb, W. E. jr., Phys. Rev. **A134**, 1429 (1964).
19. Murray, J. D., "Mathematical Biology" (Springer-Verlag, Berlin Heidelberg, 1989).
20. Vorontsov, M. A., Kirakosyan, M. E. and Larichev, A. V., Sov. J. Quant. Electron. **21**, 105 (1991).